

# Emergent collective chemotaxis without single-cell gradient sensing

Brian A. Camley,<sup>1</sup> Juliane Zimmermann,<sup>2</sup> Herbert Levine,<sup>2,3</sup> and Wouter-Jan Rappel<sup>1</sup>

<sup>1</sup>*Department of Physics, University of California, San Diego, La Jolla CA 92093*

<sup>2</sup>*Center for Theoretical Biological Physics, Rice University, Houston, TX*

<sup>3</sup>*Department of Bioengineering, Rice University, Houston, TX*

Many eukaryotic cells chemotax, sensing and following chemical gradients. However, even if single cells do not chemotax significantly, small clusters may still follow a gradient; this behavior is observed in neural crest cells and during border cell migration in *Drosophila*, but its origin remains puzzling. Here, we study this “collective guidance” analytically and computationally. We show collective chemotaxis can exist without single-cell chemotaxis if contact inhibition of locomotion (CIL), where cells polarize away from cell-cell contact, is regulated by the chemoattractant. We present explicit formulas for how cluster velocity and chemotactic index depend on the number and organization of cells in the cluster. Pairs of cells will have velocities that are strongly dependent on the cell pair’s orientation: this provides a simple test for the presence of collective guidance in neural crest cells and other systems. We also study cluster-level adaptation, amplification, and cohesion via co-attraction.

## INTRODUCTION

Cells often perform chemotaxis, detecting and moving toward increasing concentrations of a chemoattractant, to find nutrients or reach a targeted location. This is a fundamental aspect of biological processes from immune response to development. Many single eukaryotic cells sense gradients by measuring how a chemoattractant varies over their length [1]; bacteria measure chemoattractant signal over time [2]. In both, single cells are capable of net motion in the direction of higher chemoattractant. Recent measurements of the response of neural crest cells to the chemoattractant Sdf1 suggest that single neural crest cells do not significantly chemotax, but small clusters do [3]; clusters of lymphocytes may even chemotax in the opposite direction to single cells [4]. In addition, late border cell migration in the *Drosophila* egg chamber may be driven by a similar “collective guidance” mechanism where cells in a cluster migrate via whole-cell-level responses to chemoattractant [5–8]. These experimental results suggest that gradient sensing in a cluster of cells may be an *emergent* property of the cell-cell interactions, rather than arising from amplifying a single cell’s biased motion; interestingly, some fish schools also display emergent gradient sensing [9]. These topics have an important health relevance in collective cancer motility, as recent experiments suggest that tumor cell clusters are particularly effective metastatic agents [10].

In this work, we model cell clusters that chemotax collectively, show that single-cell gradient sensing is not required, and provide experimental criteria to distinguish between chemotaxis via collective guidance and other effects. We posit that individual cells cannot sense the local chemoattractant gradient, but change their interactions in response to the local level of chemoattractant. Within this model, single cells do not chemotax. We include physical interactions between cells (volume exclusion and cell-cell adhesion) and contact inhibition of loco-

motion (CIL) [11–15], in which cells polarize away from cell-cell contact. With this combination, clusters develop an outward-directed polarity of graded strength, leading to biased motion in the direction of larger chemoattractant (Fig. 1). Our quantitative computational model is a realization of the qualitative idea of “collective guidance” [6]. We make analytical predictions for how cell-cell interactions lead to emergent gradient sensing, providing a “mobility matrix” that determines the chemotactic response of a cluster. We generalize our approach with a local excitation, global inhibition (LEGI) gradient sensing mechanism [16] that can ensure perfect adaptation to different signal levels, and illustrate the consequences of adaptation for cluster chemotaxis. Though in many of our calculations, we assume strong adhesion between cells, which allows us to derive exact analytical results, we also show that this collective guidance mechanism can be effective when cell contacts are transient if cohesion between cells is driven by a long range “co-attraction” as is the case in neural crest [17].

Our model provides explicit predictions that are relatively straightforward to test experimentally, especially focusing on the behavior of pairs of cells undergoing collective guidance. This creates a framework for distinguishing collective guidance from other mechanisms where clusters gain improvement over single-cell migration, e.g. “many wrongs” averaging out error [18].

## RESULTS

### Model

We use a two-dimensional stochastic particle model to describe cells exposed to a chemical gradient  $S(\mathbf{r})$ , using the experiments of [3] on neural crest cells as a guide. We describe each cell  $i$  with a position  $\mathbf{r}^i$  and a polarity  $\mathbf{p}^i$ . The cell polarity indicates its direction and popul-

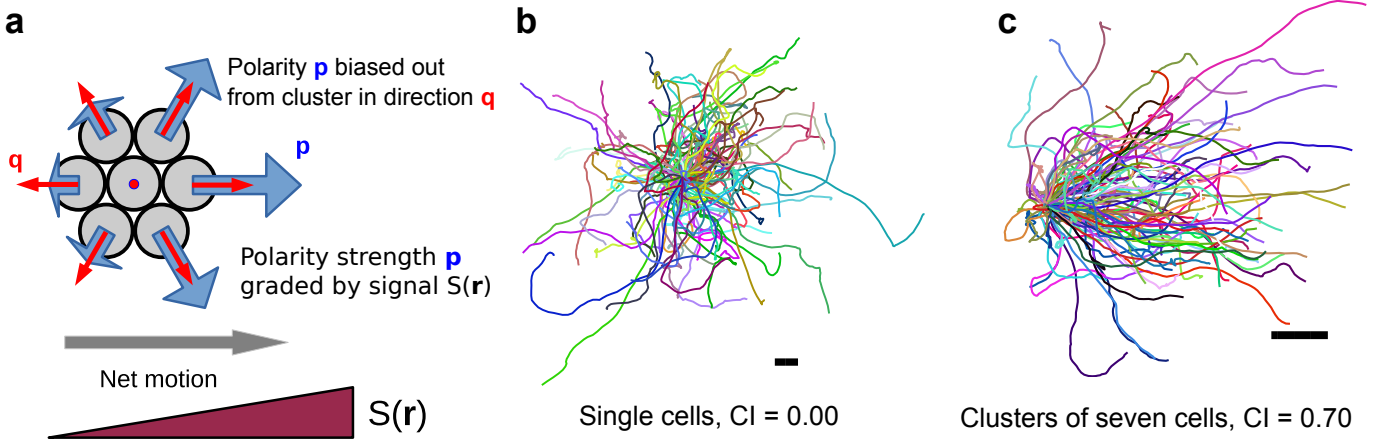


FIG. 1. **Signal-dependent contact inhibition of locomotion creates directed motion.** **a**, Schematic picture of model and origin of directed motion. Cell polarities are biased away from the cluster toward the direction  $\mathbf{q}^i = \sum_{j \sim i} \hat{\mathbf{r}}^{ij}$  by contact inhibition of locomotion (see text); the strength of this bias is graded by the local chemoattractant value  $S(\mathbf{r})$ . **b**, One hundred trajectories of a single cell and **c**, cluster of seven cells. Trajectories are six persistence times in length (120 min). Scalebar is one cell diameter. The gradient strength is  $|\nabla S| = 0.025$  in these simulations, with the gradient in the  $x$  direction.

sion strength: an isolated cell with polarity  $\mathbf{p}^i$  will travel with velocity  $\mathbf{p}^i$ . We will assume that physical forces like cell-cell adhesion and exclusion change the cell's velocity, while chemically-induced effects like CIL alter its biochemical polarity  $\mathbf{p}^i$ ; this aspect of our model could easily be generalized. Our model is:

$$\partial_t \mathbf{r}^i = \mathbf{p}^i + \sum_{j \neq i} \mathbf{F}^{ij} \quad (1)$$

$$\partial_t \mathbf{p}^i = -\frac{1}{\tau} \mathbf{p}^i + \sigma \boldsymbol{\xi}^i(t) + \beta^i \sum_{j \sim i} \hat{\mathbf{r}}^{ij} \quad (2)$$

where  $\mathbf{F}^{ij}$  are the intercellular forces, which include cell-cell adhesion and volume exclusion (see *Methods*), and  $\boldsymbol{\xi}^i(t)$  are Gaussian Langevin noises,  $\langle \xi_\mu^i(t) \xi_\nu^j(t') \rangle = 2\delta_{\mu\nu} \delta^{ij} \delta(t-t')$ , where the Greek indices  $\mu, \nu$  run over the dimensions  $x, y$ . The first two terms on the right of Eq. 2 are a standard Ornstein-Uhlenbeck model [19, 20]:  $\mathbf{p}^i$  relaxes to zero with a timescale  $\tau$ , but is driven away from zero by a fluctuating noise  $\boldsymbol{\xi}(t)$ . The last term on the right of Eq. 2 models contact inhibition of locomotion (CIL): the cell's polarity is biased away from nearby cells and toward the direction  $\mathbf{q}^i = \sum_{j \sim i} \hat{\mathbf{r}}^{ij}$ , where  $\hat{\mathbf{r}}^{ij} = (\mathbf{r}^i - \mathbf{r}^j)/|\mathbf{r}^i - \mathbf{r}^j|$  is the unit vector pointing from cell  $j$  to cell  $i$  and the sum over  $j \sim i$  indicates the sum over the neighbors of  $i$  (those cells close enough to  $i$  that  $\mathbf{F}^{ij} \neq 0$ ; see *Methods*).

For cells along the cluster edge,  $\mathbf{q}^i$  points outward from the cluster, but for interior cells  $\mathbf{q}^i$  is typically smaller or zero (Fig. 1a). Cells around the edge are strongly polarized away from the cluster, while interior cells have weaker protrusions, as observed by [3]. We model the chemical  $S(\mathbf{r})$  as changing a cell's susceptibil-

ity to CIL,  $\beta^i, \beta^i = \bar{\beta}S(\mathbf{r})$ . This models the result of [3] that the chemoattractant Sdf1 stabilizes protrusions induced by CIL [3]. If CIL is present even in the absence of chemoattractant ( $S = 0$ ), as in neural crest [3], i.e.  $\beta^i = \beta_0 + \bar{\beta}S(\mathbf{r})$ , this will not significantly change our analysis. Similar results can also be obtained by assuming that all protrusions are stabilized by Sdf1 ( $\tau$  regulated by  $S$ ), though with some complications (*Appendix*, Fig. A1). We also note that recent experiments on breast cancer cells also support the idea that there is an interaction between chemoattractants and CIL [21].

### Cluster motion and chemotactic efficiency depend on cluster size and shape

Our model predicts that while single cells cannot chemotax, clusters as small as two cells will, consistent with experiment [3]. The simplicity of Eqs. 1-2 allows analytical predictions for how cluster chemotaxis depends on the number and configuration of cells.

Eq. 1 states that, in our units, the velocity of a single cell is equal to the force on it (i.e. the mobility is one). For a rigid cluster of  $N$  cells, then the mean velocity of the cluster will be  $1/N$  times the total force on the cluster. As  $\mathbf{F}^{ij} = -\mathbf{F}^{ji}$ , the cluster velocity is  $\mathbf{V} = N^{-1} \sum_i \mathbf{p}^i$ . When the cluster configuration changes slowly over the timescale  $\tau$ , Eq. 2 can be treated as an Ornstein-Uhlenbeck equation with an effectively time-independent bias from CIL. The mean polarity is then  $\langle \mathbf{p}^i \rangle = \beta^i \tau \sum_{j \sim i} \hat{\mathbf{r}}^{ij}$ , with Gaussian fluctuations away from the mean,  $\langle (\mathbf{p}_\mu^i - \langle \mathbf{p}_\mu^i \rangle)^2 \rangle = \sigma^2 \tau$ .

The mean velocity of a cell cluster is then

$$\langle \mathbf{V} \rangle_c = \frac{\bar{\beta}\tau}{N} \sum_i S(\mathbf{r}^i) \sum_{j \sim i} \hat{\mathbf{r}}^{ij} \quad (3)$$

where  $\langle \dots \rangle_c$  indicates an average over the fluctuating  $\mathbf{p}^i$  but with a fixed configuration of cells  $\mathbf{r}^i$ . In a constant chemoattractant field,  $S = S_0$ , no net motion is observed, as  $\sum_i \sum_{j \sim i} \hat{\mathbf{r}}^{ij} = 0$ . For linear or slowly-varying gradients  $S(\mathbf{r}) \approx S_0 + \mathbf{r} \cdot \nabla S$ ,

$$\langle \mathbf{V} \rangle_c \approx \bar{\beta}\tau \mathcal{M} \cdot \nabla S \quad (4)$$

where the matrix  $\mathcal{M}$  only depends on the cells' configuration,

$$\mathcal{M}_{\mu\nu} = \frac{1}{N} \sum_i q_{\mu}^i r_{\nu}^i \quad (5)$$

where, as above,  $\mathbf{q}^i = \sum_{j \sim i} \hat{\mathbf{r}}^{ij}$ . Eq. 4 resembles the equation of motion for an arbitrarily shaped object in a low Reynolds number fluid under a constant force  $\bar{\beta}\tau \nabla S$  [22]: by analogy, we will call  $\mathcal{M}$  the ‘‘mobility matrix.’’ There is, however, no fluctuation-dissipation relationship as there would be in equilibrium [23].

Within our model, a cluster's motion can be highly anisotropic. Consider a pair of cells separated by unit distance along the direction  $(\cos \theta, \sin \theta)$ . Then by Eq. 5,  $\mathcal{M}_{xx} = \frac{1}{2} \cos^2 \theta$ ,  $\mathcal{M}_{xy} = \mathcal{M}_{yx} = \frac{1}{2} \cos \theta \sin \theta$ ,  $\mathcal{M}_{yy} = \frac{1}{2} \sin^2 \theta$ . Therefore, if the gradient is in the  $x$  direction, we expect  $\langle V_x \rangle_c = \frac{V_0}{2} \cos^2 \theta$  and  $\langle V_y \rangle_c = \frac{V_0}{2} \cos \theta \sin \theta$ , where  $V_0 = \bar{\beta}\tau |\nabla S|$ . Cell pairs move in the direction of the chemoattractant, but their net motion is constrained to be along the pair axis – there can be a transient bias in the  $y$  direction before the cell pair reorients due to fluctuations in  $\mathbf{p}^i$  (Fig. 2). We compare our theory for the motility of rigid cell clusters (Eq. 4) with a simulation of the stochastic model of Eq. 1-2 with strongly adherent cell pairs with excellent agreement (Fig. 2).

We can also analytically compute  $\mathcal{M}$  and hence velocity for larger clusters (Table I, *Appendix*, Fig. A2). For a cluster with  $Q$  layers of cells surrounding a center cell, we find  $\mathcal{M}_{\mu\nu} = f(Q) \delta_{\mu\nu}$ , with  $f(Q) = \frac{9Q^2 + 3Q}{2 + 6Q + 6Q^2}$ . A cluster with  $Q$  layers has  $N = 1 + 3Q + 3Q^2$  cells; thus the mean velocity of a  $Q$ -layer cluster is given by  $\langle V_x \rangle_c / V_0 = \bar{\mathcal{M}} = \frac{3N - \sqrt{12N - 3}}{2N}$ , where  $\bar{\mathcal{M}} = \frac{1}{2} (\mathcal{M}_{xx} + \mathcal{M}_{yy})$ . This is confirmed by simulations of the full model (Fig. 3a). We note that  $\langle V_x \rangle_c$  is an average over all times, and hence orientations (see below, *Appendix*).

Theveneau et al. [3] find that small clusters of neural crest cells chemotax efficiently, as indicated by chemotactic index. Chemotactic index measures the effectiveness of a biased random motion, and is commonly defined as the ratio of the distance the object travels in the direction of the gradient (the  $x$  displacement) to its total distanced traveled [24];  $CI$  ranges from -1 to 1. When averaging over multiple trajectories we define  $CI \equiv \langle V_x \rangle_c / \langle |\mathbf{V}| \rangle_c$ ,

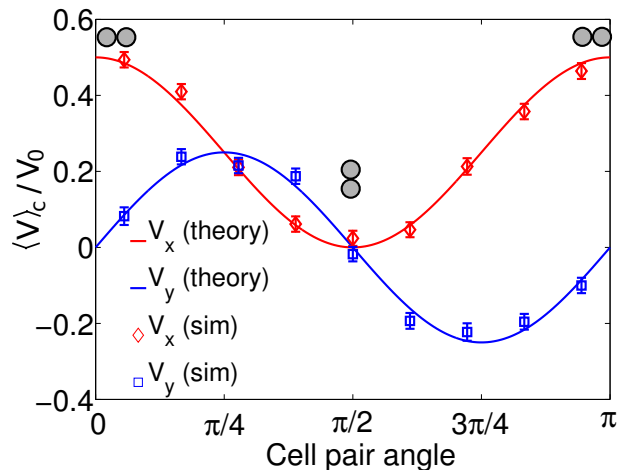


FIG. 2. **Adherent pairs of cells undergo highly anisotropic chemotaxis.** The average chemotactic velocity of a highly adherent cell pair  $\langle V_x \rangle_c$  depends strongly on the angle  $\theta$  between the cell-cell axis and the chemotactic gradient. Cell pairs also develop a transient drift velocity perpendicular to the direction of chemotaxis  $\langle V_y \rangle_c$ , which also depends on cell pair orientation.  $V_0 \equiv \bar{\beta}\tau |\nabla S|$  is the scale of the velocity. Simulations are of Eqs. 1-2, allowing the cell pair to rotate from the fluctuations in  $\mathbf{p}^i$ . We compute  $\langle V_\mu \rangle_c$  by tracking the instantaneous angle, then averaging over all velocities within the appropriate angle bin. Error bars are one standard deviation of the mean, calculated from a bootstrap over  $n = 13,000$  trajectories of  $6\tau$  (120 minutes) each.

where the average is over both time and trajectories (and hence over orientation). Within our model, for a given  $|\nabla S|$ , both chemotactic index and mean velocity quickly increase with the number of cells (Fig. 3, Table I), then saturate, with the chemotactic index saturating at 1.

Both chemotactic velocity  $\langle V_x \rangle_c$  and chemotactic index  $CI$  may be computed analytically.  $\mathbf{V}$  has mean  $\langle \mathbf{V} \rangle_c$  given by the orientational average of Eq. 4, and variance  $\langle (V_x - \langle V_x \rangle_c)^2 \rangle = \langle (V_y - \langle V_y \rangle_c)^2 \rangle = \sigma^2 \tau / N$ . In our model,  $CI$  only depends on the ratio  $c$  of the mean chemotactic velocity to its standard deviation,

$$CI = \frac{\langle V_x \rangle_c}{\sqrt{\langle (V_x - \langle V_x \rangle_c)^2 \rangle}} = \frac{\bar{\beta}\tau \bar{\mathcal{M}} |\nabla S|}{\sigma \sqrt{\tau / N}} \quad (6)$$

where  $L_{1/2}$  is a generalized Laguerre polynomial. When the mean cluster velocity is much larger than the fluctuations in cluster velocity,  $c \gg 1$  and thus  $CI \rightarrow 1$ , and when fluctuations are large,  $|c| \ll 1$ ,  $CI \rightarrow 0$  (*Appendix*, Fig. A3). Together, Eq. 4, Eq. 6 and Table I provide a complete analytic prediction for cluster velocity and chemotactic index, and we observe excellent agreement with our simulations (Fig. 3).

We note that mean velocity only depends on the cluster configuration and  $V_0 = \bar{\beta}\tau |\nabla S|$ , so by rescaling ve-


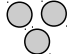
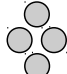
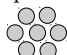
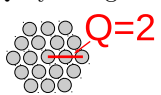
Shape	$\mathcal{M}$	Angularly averaged $\overline{\mathcal{M}}$
Dimer 	$\begin{pmatrix} 1/2 & 0 \\ 0 & 0 \end{pmatrix}$	1/4
Trimer 	$\begin{pmatrix} 1/2 & 0 \\ 0 & 1/2 \end{pmatrix}$	1/2
Tetramer 	$\begin{pmatrix} 1/2 & 0 \\ 0 & 3/4 \end{pmatrix}$	5/8
Heptamer 	$\begin{pmatrix} 6/7 & 0 \\ 0 & 6/7 \end{pmatrix}$	6/7
Q-layer oligomer 	$\begin{pmatrix} f(Q) & 0 \\ 0 & f(Q) \end{pmatrix}$	$f(Q) \equiv \frac{9Q^2+3Q}{2+6Q+6Q^2}$

TABLE I. **Effective mobility matrices  $\mathcal{M}$  for several cell configurations.** For each of the configurations shown, nearest-neighbor cells are elements of a hexagonal lattice with unit spacing. In a  $Q$ -layer oligomer, there are  $N(Q) = 1 + 3Q + 3Q^2$  cells. Matrices are presented for the orientation shown in the left column; other orientations may be found by transforming the mobility tensor;  $\overline{\mathcal{M}} = \frac{1}{2}(\mathcal{M}_{xx} + \mathcal{M}_{yy})$  (*Appendix*).

locities by  $V_0$ , the mean velocity as a function of  $N$  for many different gradient strengths collapses onto a single curve (Fig. 3a). The rate at which  $CI$  increases depends on the gradient strength  $|\nabla S|$  and noise strength  $\sigma$  (Eq. 6, Fig. 3b).

We can understand why the mean velocity saturates by looking at the limit of a large, circular cluster of radius  $R$ . Here, we expect  $\mathbf{q}^i = a\hat{\mathbf{n}}$  on the outside edge, where  $a$  is a geometric prefactor and  $\hat{\mathbf{n}}$  is the outward normal, with  $\mathbf{q}^i = \mathbf{0}$  elsewhere. In this limit,  $\mathcal{M}_{\mu\nu} \sim \frac{a}{\pi R^2} \int_0^{2\pi} (Rd\theta) \hat{\mathbf{n}}_\mu(\theta) \mathbf{r}_\nu = 2a\delta_{\mu\nu}$ , which is independent of cluster radius  $R$ . A related result has been derived for circular clusters by Malet-Engra et al. [4]; we note that they do not consider the behavior of single cells or small numbers of cells.

We also note that, in our model, sufficiently asymmetric clusters can rotate. Under assumptions similar to Eq. 4 above, clusters will have a mean angular velocity proportional to  $\mathbf{A} \cdot \nabla S$ , where  $\mathbf{A}$  is a vector depending only on the cluster geometry. This is once again similar to the sedimentation of a particle of general shape in a low Reynolds number flow [22]. However, for clusters in Table I,  $\mathbf{A} = \mathbf{0}$  and they will not rotate in a linear gradient. If  $\mathbf{A} \neq \mathbf{0}$ , clusters rotate to a fixed angle with respect to the gradient direction; there is no persistent rotation in a linear gradient (*Appendix*). We note, however, that in nonlinear gradients, persistent rotation of sufficiently asymmetric clusters may be induced.

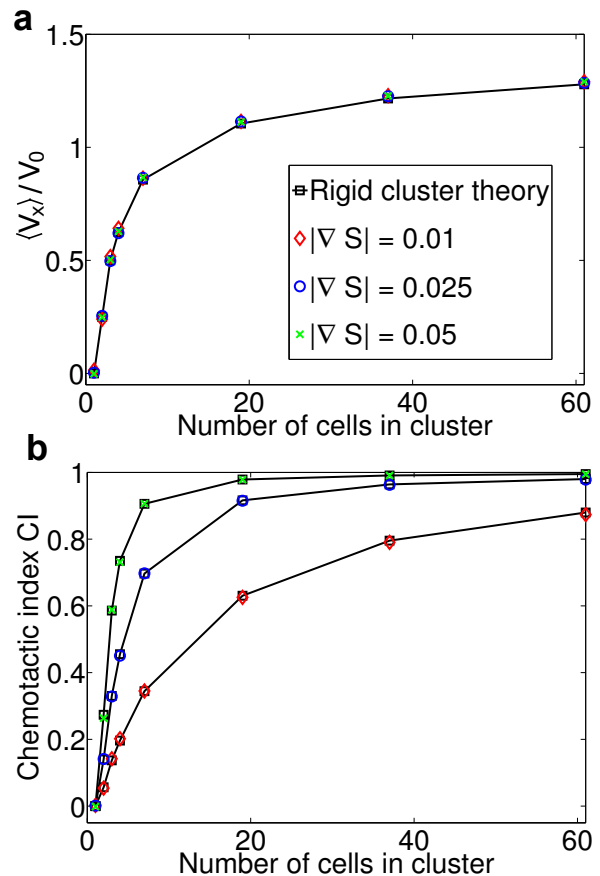


FIG. 3. **Larger cell clusters chemotax more effectively, but their velocity saturates a.** As the number of cells  $N$  in a cluster increases, the mean velocity  $\langle V_x \rangle$  increases with  $N$  but then saturates; the mean velocity can be collapsed onto a single curve by rescaling by the velocity scale  $V_0 \equiv \beta\tau|\nabla S|$ . **b.** The chemotactic index  $CI$  also saturates to its maximum value. Black squares and lines are “rigid cluster theory” – the orientationally-averaged drift velocity computed for rigid clusters by Eq. 4 and Eq. 6. Colored symbols are simulations of the full model with strong adhesion interactions as discussed in *Methods*. We note that, in addition to number, cell cluster shape may influence  $\langle V_x \rangle$  (*Appendix Fig. A4*); our calculations and simulations are for the shapes shown here and in Table I. Error bars on this figure are the symbol size or smaller;  $n \geq 2000$  trajectories of  $6\tau$  are used for each point.

Our result for cluster velocity, Eq. 5, is strongly dependent on the assumed linear profile of  $S(x)$  and hence  $\beta^i$  across the cluster – larger clusters have a larger total change in  $\beta^i$ . If the cell is in a nonlinear  $S(\mathbf{r})$  or the gradient of  $S(\mathbf{r})$  is amplified,  $\langle V_x \rangle$  as a function of  $N$  will change, which we show explicitly in the next section.

**Adaptation and amplification can create  
non-monotonic dependences of velocity on cluster  
size**

In the model we have studied so far, for clusters to move efficiently, we must have  $\beta^i$  large enough so that the change in  $\beta^i$  across the cluster can drive movement. However, if  $\beta^i$  becomes too large, CIL will overcome cell-cell adhesion and the cluster will scatter (Fig. 4a). Scattering happens naturally as the cluster travels up a chemoattractant gradient, increasing  $\beta^i$ , but if  $\beta^i$  adapts to the strength of  $S$ , scattering may be avoided. Many cellular responses undergo adaptation, where the response to a signal returns to a baseline level when exposed to a persistently elevated signal [16, 25, 26]; adaptation can also allow for easier amplification of a shallow signal. How can individual cells adapt while maintaining a graded response across the cluster? One answer comes from gradient sensing in single eukaryotic cells: a local excitation, global inhibition (LEGI) model [1, 16, 27, 28]. We generalize LEGI to cell clusters and show that it creates adaptation and gradient sensing. In this LEGI model, signal  $S$  produces chemicals  $A$  and  $I$  within each cell.  $A$  remains localized within each cell, but  $I$  can be transferred between contacting cells with rate  $k_D$ .  $A$  upregulates and  $I$  downregulates the final output,  $R$ , which we assume controls CIL,  $\beta = \bar{\beta}g(R)$  (Fig. 4b). Our model, which generalizes [16] to clusters, is:

$$\partial_t A^i = k_A S(\mathbf{r}^i) - k_{-A} A^i \quad (7)$$

$$\partial_t I^i = k_I S(\mathbf{r}^i) - k_{-I} I^i - k_D n^i I^i + k_D \sum_{j \sim i} I^j \quad (8)$$

$$\partial_t R^i = k_R A^i (1 - R^i) - k_{-R} I^i R^i \quad (9)$$

where  $n^i$  is the number of neighbors to the  $i^{\text{th}}$  cell. Eq. 8 is a reaction-diffusion model on the network of cells [29, 30]. Assuming diffusive transfer between contacting cells is appropriate if the inhibitor  $I$  is transferred from one cell's cytosol to the other, e.g. by gap junctions. Gap junctions modulate neural crest cell motility *in vivo* [31, 32], making this plausible, though no diffusing inhibitor has yet been identified. If gap junctions do not form quickly enough, it may be possible to create adaptation by extracellular secretions, similar to the processes involved in quorum sensing in bacteria [33] or via "transcytosis" [34].

The LEGI model of Eqs. 7-9 perfectly adapts to changing uniform signals [16]. We find its steady state,  $A^{i,ss} = \frac{k_A}{k_{-A}} S^i$  and  $R^{i,ss} = \frac{A^i/I^i}{A^i/I^i + k_{-R}/k_R} \approx \frac{k_R}{k_{-R}} \frac{A^i}{I^i}$ , where the approximation holds for  $k_{-R} \gg k_R$ . For a signal that is constant in space  $S(x) = S_0$ ,  $I^{i,ss} = \frac{k_I}{k_{-I}} S_0$ , and thus the steady state  $R^{i,ss}(t)$  is independent of  $S_0$ . If  $S_0$  changes over time,  $R$  first increases and then adapts to its steady-state value, as do the cell polarities (Fig. 4c).

The LEGI scheme can also adapt to gradients in  $S(\mathbf{r})$ . In the limit of fast intercellular diffusion ( $k_D \gg k_{-I}$ ) in a connected cluster,  $I^{i,ss} \approx \frac{k_I}{k_{-I}} \bar{S}$ , where  $\bar{S} = N^{-1} \sum_i S^i$  is the mean signal over the cluster (*Appendix*). In this limit and  $k_{-R} \gg k_R$ ,

$$R^{i,ss} \approx \frac{k_R}{k_{-R}} \frac{k_A}{k_{-A}} \frac{k_{-I}}{k_I} \frac{S(\mathbf{r}^i)}{\bar{S}} \equiv R_0 \frac{S(\mathbf{r}^i)}{\bar{S}} \quad (10)$$

Under these assumptions,  $R^i$  develops a profile across the cell proportional to the percentage change in the signal  $S(\mathbf{r})$  across the cell. In this limit, if  $\beta^i = \bar{\beta} R^i/R_0$ , our results from above will be rescaled,  $\nabla S \rightarrow \nabla S/\bar{S}$  in Eq. 4 and Eq. 6. Adapting clusters in a linear gradient will no longer have a constant speed and chemotactic index. For this reason, we study adaptation in an exponential gradient,  $S(x) = S_0 e^{x/S_1}$  so that  $\nabla S/\bar{S} \approx S_1$  is constant (as in [24]).

What constraints do gap junction kinetics place on this mechanism? Gap junction transfer times are of the order of a few minutes [35]; we estimate  $k_D \approx 0.2 \text{ min}^{-1}$  ( $k_D = 4$  in our units). For effective gradient sensing,  $I$  must equilibrate over the cluster within the timescale  $1/k_{-I}$ , i.e.  $\alpha \equiv k_{-I}/k_D \ll 1/N$  (*Appendix*). Lower  $\alpha$  improves gradient sensing (Fig. 4d), but  $k_{-I}$  cannot be decreased arbitrarily: if  $k_{-I} \ll \tau^{-1}$ ,  $R$  will not reach a steady state over the relevant timescale for cell polarity. We expect  $k_{-I} \geq \tau^{-1}$ , i.e.  $\alpha \geq 0.25$ . If this is true, clusters have imperfect gradient sensing:  $R$  becomes shallower and nonlinear in larger clusters (Fig. 4d). When this occurs, cluster velocities change. For  $\alpha = 0.25$ , mean cluster velocities are non-monotonic in  $N$ , with a maximum at  $N = 19$ . This optimum size can be controlled by changing  $\alpha$  (Fig. 4e). Non-monotonicity can make comparison to experiment difficult; [3] report values for "small" and "large" clusters, which could depend significantly on the critical cluster size. Detailed measurements as a function of the cluster radius [4] may be necessary.

Within chemotaxing single cells, small differences in signal are amplified to large differences in behavior between the cell front and back, allowing efficient migration in shallow chemotactic gradients [1, 16, 36]. Amplification can also increase cluster motility. Clusters move via a tug-of-war mechanism – back cells oppose the net motion of the cluster (Fig. 1); if these back cells are suppressed, cluster velocity increases. We treat an illustrative but extreme example of amplification in which a cell's response is switchlike, with front cells strongly polarized and back cells suppressed,  $\beta^i = \bar{\beta}g(R/R_0)$ , with  $g(x) = \frac{1}{2} [1 + \tanh(x-1)/\xi]$ . For  $\xi \ll 1$ ,  $\beta^i \approx \bar{\beta}$  where  $R^i > R_0$  (cluster front), and  $\beta^i \approx 0$  if  $R^i < R_0$  (cluster back). This switchlike response means that the precise value of  $R$  is not as crucial as whether it is greater or larger than  $R_0$ . For this reason, with strong amplification ( $\xi = 10^{-2}$ ), cluster velocity is, assuming a steady state of  $R^i$ , much less sensitive to the intercluster diffusion rate  $k_D$  (Fig. 4f). However, the assumption that  $R^i$

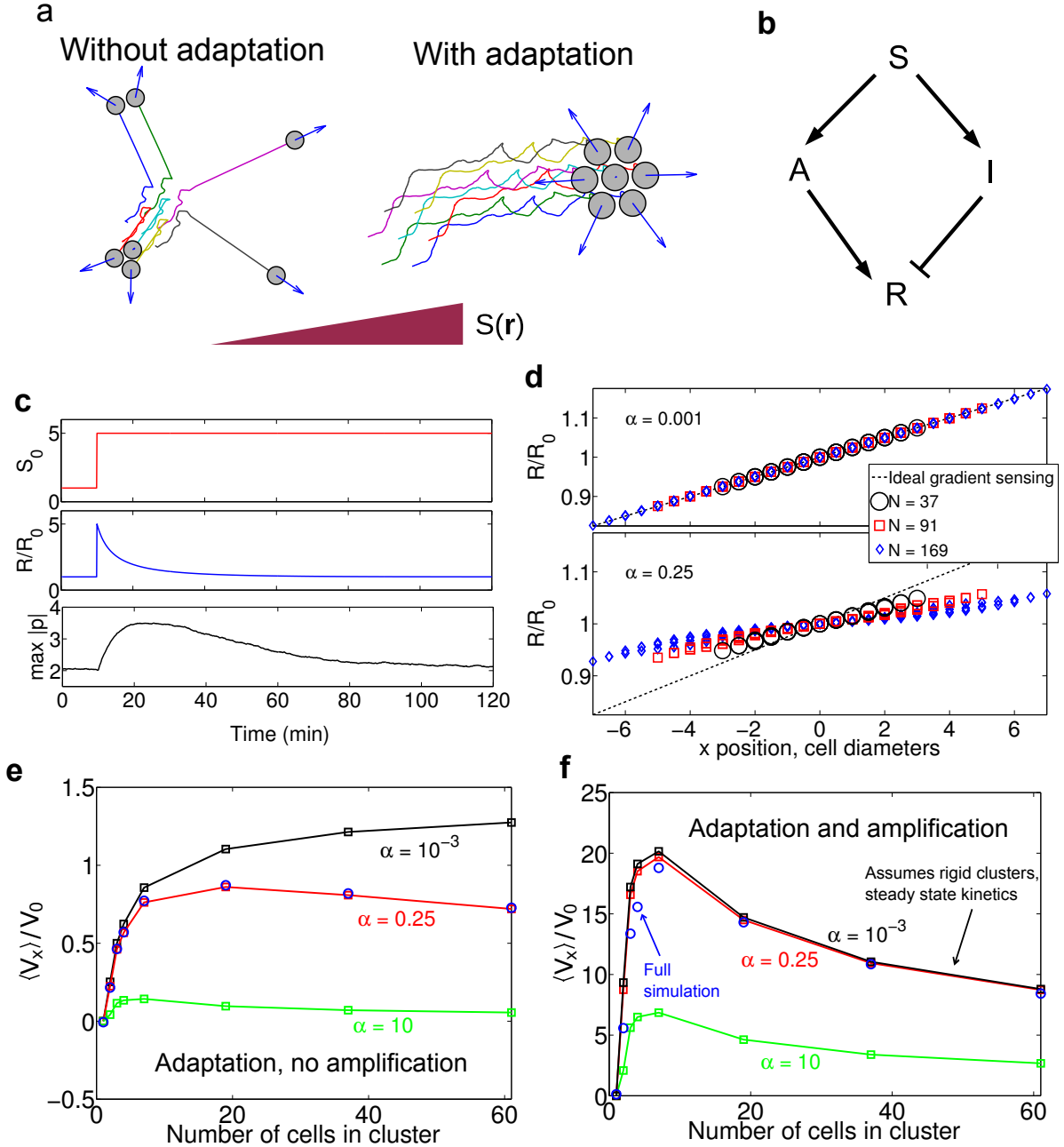


FIG. 4. **Adaptation and amplification can change cluster mobility properties.** **a**, Weakly adherent clusters without adaptation scatter as they move up the gradient, but those that adapt do not;  $v_a = v_r = 23$  in this simulation (*Methods*). Arrows are polarity  $\mathbf{p}^i$ . **b**, Schematic picture of LEGI model of Eqs. 7-9. **c**, Adaptation of  $R$  (same for all cells) and maximum  $|\mathbf{p}^i|$  to a step in uniform signal strength  $S_0$ .  $R_0 = \frac{k_R}{k_{-R}} \frac{k_A}{k_{-A}} \frac{k_{-I}}{k_I}$  is the scale of  $R$  and we assume  $\beta^i = \bar{\beta} R^i / R_0$ . **d**,  $R^{ss}$  on clusters of different sizes shown for  $\alpha = k_{-I}/k_D = 0.25$  (plausible for gap junction transfer), and  $\alpha = 10^{-3}$  (near-ideal). Dashed line shows the ideal result  $R^{ss} = R_0 S(x) / \bar{S}$ . **e**, Imperfect LEGI gradient sensing creates an optimum cluster size. **f**, Amplification also creates an optimal cluster size, but weakens the dependence on  $\alpha$  and can strongly increase cluster velocity.  $\bar{\beta} = 0.2$  in **f** – larger values of  $\bar{\beta}$  can lead to larger deviations from steady-state results. In **e** and **f**, squares and lines are results assuming rigid clusters and that Eq. 7-9 are at their steady state, while blue circles are full simulations including the reaction dynamics.  $V_0 \equiv \bar{\beta} \tau S_1 / S_0$  is the scale of the velocity. The simulations in **e** and **f** are in an exponential gradient,  $S(x) = S_0 e^{S_1 x}$ ,  $S_0 = 1$ ,  $S_1 = 0.025$ , and have error bars of the symbol size or smaller;  $n \geq 2000$  trajectories of  $6\tau$  are used for each point.

is at its steady state is not necessarily perfect for amplified clusters; fluctuating  $R^i$  coupled with the nonlinear dependence of  $\beta^i$  on  $R^i$  above can lead to deviations from the steady-state result (Fig. 4f, blue circles).

With amplification, cluster velocity increases beyond its usual scale of  $V_0$ , as the cluster is no longer engaged in a tug-of-war. However, cluster velocity is still non-monotonic in cluster size, decreasing as  $N^{-1/2}$  at large  $N$ , as expected from balancing edge-driven motion with the friction of the whole cluster (Fig. 4f). Other possibilities for amplification (e.g.  $\beta^i = \beta(R^i/R_0)^2$  [16]) lead to different behaviors for  $\langle V_x \rangle$  as a function of  $N$ .

### Loosely bound clusters mediated by co-attraction can also effectively chemotax, but may rotate

Until this point, we have only looked at highly adherent, effectively rigid clusters, where analytic results are possible. However, collective cell migration can also occur with a high degree of fluidity and with many cell-cell rearrangements [37–43]. In addition, we have until now assumed that the only attraction between cells is short-range, representing cell-cell adhesion. However, neural crest cells also attract one another through chemical secretions, which can control the extent of cluster directionality and cohesion [17, 44]. We extend our model to allow for this possibility, and show that clusters of cells that cohere via co-attraction can also be directed by collective guidance as we have modeled here. These clusters need not be rigid, and can have significant re-arrangement or even only transient contacts.

To model co-attraction, we assume that each cell secretes a co-attractant  $c$ , which diffuses through the extracellular medium with diffusion coefficient  $D$  and degrades with rate  $k_c$ . We model co-attraction by adding an additional term to Eq. 2 encouraging cells to polarize toward higher  $c$ ,

$$\partial_t \mathbf{p}^i = -\frac{1}{\tau} \mathbf{p}^i + \sigma \boldsymbol{\xi}^i(t) + \beta^i \sum_{j \sim i} \hat{\mathbf{r}}^{ij} + \chi \frac{\nabla c(\mathbf{r}^i)}{|\nabla c|} \Theta(|\nabla c| - g_0) \quad (11)$$

where  $\Theta(x)$  is the Heaviside step function,  $\Theta(x) = 0$  for  $x < 0$  and  $\Theta(x) = 1$  for  $x > 0$ . This term biases cells to polarize toward increasing  $c$ , but assumes the strength of this chemotaxis to  $c$  is independent of the gradient strength, once the gradient strength is above the threshold  $g_0$ . The saturation of polarization is supported by recent experiments in T cells [45]; modifying this assumption would change how coherent groups of differing numbers of cells are. We will turn off physical cell-cell adhesion in our simulations with co-attraction ( $v_a = 0$ ), but CIL still acts between cells within a distance of  $D_0 = 1.2$  cell diameters, as above.

The gradient at the position  $\mathbf{r}^i$ ,  $\nabla c(\mathbf{r}^i)$ , is computed under the assumption that secretion, degradation, and diffusion of  $c$  are much faster than all other processes in our model [44], and is found to be (*Appendix*)

$$\nabla c(\mathbf{r}^i) = - \sum_{j \neq i} K_1(|\mathbf{r}^i - \mathbf{r}^j|/\ell) \hat{\mathbf{r}}^{ij} \quad (12)$$

where  $K_1(x)$  is a modified Bessel function of the second kind and the degradation length  $\ell$  is set by  $\ell^2 = D/k_c$ . We choose  $\ell$  to be five cell diameters ( $100\mu\text{m}$ ), similar to the value used by [44].

We find that cell clusters that co-attract can chemotax efficiently, even if they are only loosely bound with relatively transient interactions and a good deal of cell-cell rearrangement (Fig. 5a, Movie 1). As the degree of co-attraction increases, clusters may develop a persistent rotational motion while they chemotax (Fig. 5b, Movie 2). This is consistent with other simulations that show that self-propelled particles with long-range interactions from chemotaxis or other sources can develop a vortex state [46–48]. We show a phase diagram of the cluster chemotactic index as well as the mean angular speed in the cluster in Fig. 5c,d. The chemotactic index is generally maximized when the co-attraction strength  $\chi$  and CIL strength  $\bar{\beta}$  are similar, and can be increased by simultaneously increasing  $\chi$  and  $\bar{\beta}$ . We can understand many of these results intuitively. Increasing the co-attraction increases the number and duration of interactions, and since the chemotactic response to the signal  $S$  emerges from cell-cell interactions, thus increases chemotactic efficiency. Increasing  $\bar{\beta}$  increases the (graded) polarization of the cells due to CIL, and hence the chemotactic index – but unless  $\chi$  also increases, the increase in CIL causes the cluster density to decrease, reducing the number of interactions. However, increasing  $\chi$  to be much larger than  $\bar{\beta}$  leads to both rotation and a decreased chemotactic index. We emphasize that Fig. 5c plots the *cluster* chemotactic index; for loosely bound clusters, especially with rotation, the chemotactic index of an individual cell can be very different from that of the cluster.

The qualitative results of our minimal, rigid model are recapitulated in the model with co-attraction: larger clusters are generally faster and more efficient (Fig. 5e,f). Mean velocity increases sublinearly with cluster size, and we suspect it will saturate, though we have not yet observed this.

We note that the co-attraction simulations in Fig. 5 assume  $\beta^i = \beta S(\mathbf{r}^i)$ ; there is no LEGI adaptation mechanism. For this reason, as the cell cluster travels up the gradient, the mean value of  $\beta$  on the cluster increases, which will change the morphology and dynamics of the cluster. The value of the chemotactic index we present is averaged over the time from  $12.5\tau$  to  $50\tau$  after the simulation is initialized; changing this averaging range does not qualitatively change the results in Fig. 5.

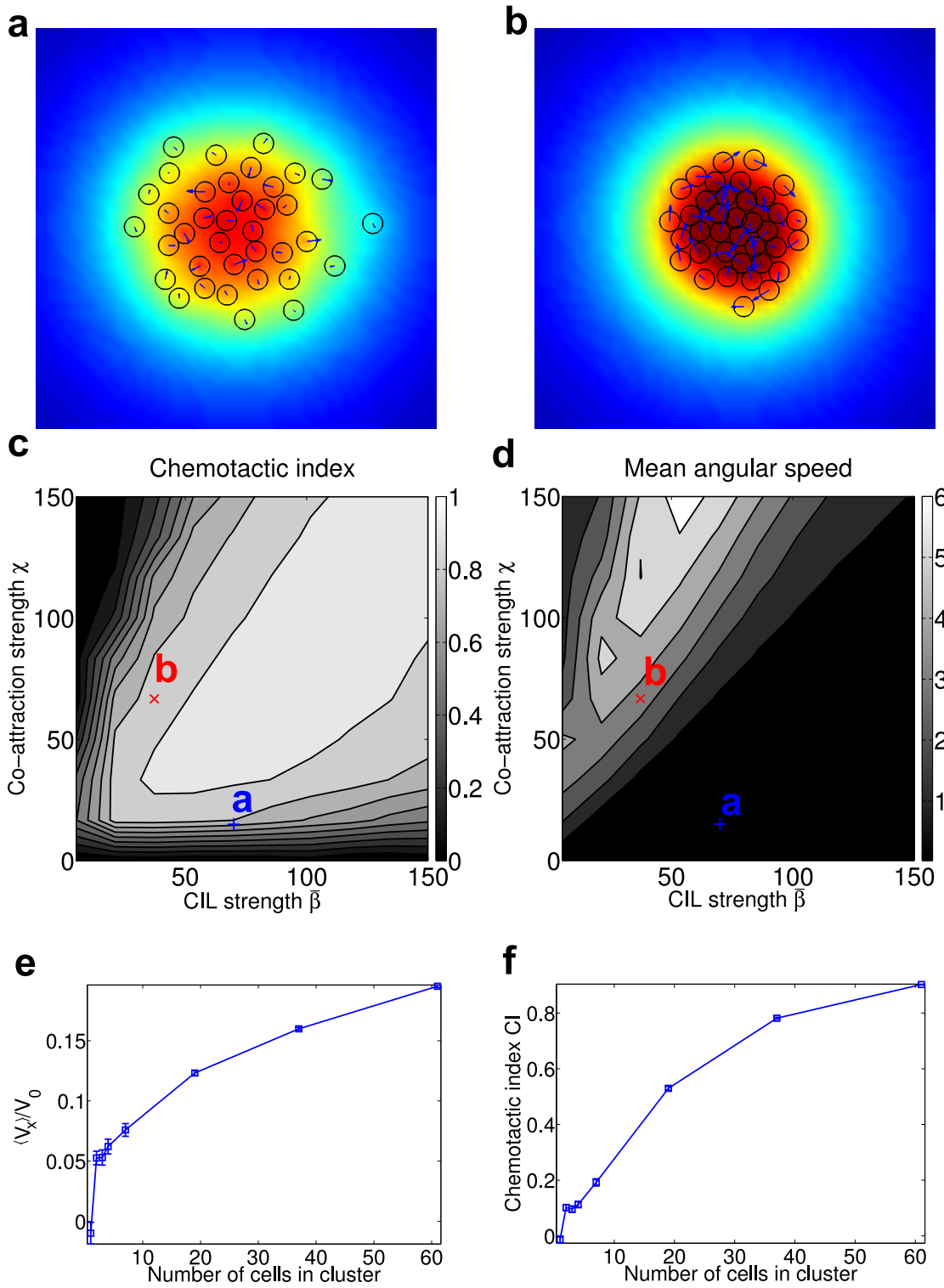


FIG. 5. **Co-attraction and graded CIL can create directed motion.** **a** is a representative snapshot of a chemotaxing cluster loosely bound by co-attraction, while **b** shows a rotating chemotaxing cluster with stronger co-attraction. In **a** and **b**, the color map is the co-attractant field  $c(\mathbf{r})$ , the blue arrows are the cell polarity  $\mathbf{p}^i$ , and the cells are drawn as black circles. **c**, Phase diagram of chemotactic index of clusters of  $N = 37$  cells. CI increases when both co-attraction  $\chi$  and CIL strength  $\beta$  are increased. **d**, Phase diagram of mean angular speed  $\langle |\Omega| \rangle$  of clusters of  $N = 37$  cells. Clusters with sufficiently high co-attraction develop rotational motion. Points corresponding to the simulations shown in **a** and **b** are marked on the phase diagrams of **c** and **d**. **e** and **f**, Cluster velocity and CI increase with increasing cluster size, as with strong co-attraction. Parameters correspond to simulation shown in **a**;  $V_0 = \beta\tau|\nabla S|$ . Throughout this figure, the degradation length  $\ell = 5$  cell diameters.  $n = 100$  trajectories of length  $50\tau$  are used for each point of the phase diagrams in **c** and **d**, which are contour plots based on a  $10 \times 10$  sample of the space  $\beta \in [5, 150]$ ,  $\chi \in [0, 150]$ .  $n = 200$  trajectories of length  $50\tau$  are used for each point in **e** and **f**.  $\Delta t = 0.005$ ,  $v_a = 0$ ,  $v_r = 100$ , and  $|\nabla S| = 0.025$ .



## DISCUSSION

### Comparison with experiment

We provide a simple, quantitative model that embodies a minimal version of the collective guidance hypothesis [3, 6] and provides a plausible initial model for collective chemotaxis when single cells do not chemotax. We show that small clusters of cells can chemotax, as observed by [3], even if single cells cannot. However, our minimal model predicts that both velocity and chemotactic index increase, then saturate with increasing cluster size – inconsistent with the results of [3], who find that both are similar between small and large clusters. Within our models that include a diffusive inhibitor, the velocity of small and large clusters can be similar. However, we predict that the cluster velocity is non-monotonic in cluster size. This implies that large clusters could have either a larger or smaller velocity than small clusters, depending on the definitions of the size categories and the details of the adaptation mechanism (e.g. the rate of diffusion of the inhibitor). More detailed experiments could identify this non-monotonicity. In addition, considering the possibility of correlated noise across the cell cluster, as discussed recently in [4], may alter the behavior of cluster chemotactic index. Our model with co-attraction also shows that, consistent with experiments on neural crest [3], that the collective guidance mechanism proposed here can guide cells even with only transient contacts.

Our model suggests that the primary driver of the dynamics of these clusters are cells at the edge. This is consistent with the observations of [3] on neural crest, who observe that only the edge cells develop strong protrusions: there are no cryptic protrusions. In other collective cell migrations, notably the classic example of monolayer MDCK migration, traction forces are also exerted significantly away from the edge [49], which we expect would significantly alter the scaling of cluster chemotactic behavior with cluster size. Ultimately, traction force measurements may be crucial in determining whether our assumption of edge-driven dynamics is appropriate; however, this assumption is consistent with the currently available data.

In this paper, we also proposed a LEGI model that allows cells and cell clusters to adapt to changing levels of chemoattractant. Adaptation in single-cell chemoresponse is a ubiquitous and well-tested principle, but its existence is not established for clusters; applying a step response would be a straightforward test of adaptation, and we would expect protrusions and traction forces to peak and then adapt (Fig. 4c). Our results suggest that in some cell types, gap-junction mediated gradient sensing across the cluster may be effective. Adaptation to and amplification of chemoattractant gradients can also create an “optimum size” for clusters, where both larger

and smaller clusters are on average slower than the optimum. We expect this slowing of larger clusters, which occurs either if adaptation is imperfect or if the chemoattractant signal is amplified, to be a relatively generic feature of tightly bound clusters. As the cluster motility is driven by the edge cells, but resisted by the bulk of the cluster, an increasingly large cluster must either slow or  $\beta^i$  at the edge must increase indefinitely. This suggests that large clusters will either slow (Fig. 4e,f) or eventually scatter as  $\beta^i$  overcomes adhesion. If clusters use the LEGI mechanism with a diffused inhibitor mediated by gap junctions, we expect cell clusters to slow.

### Possible extensions

Our stochastic interacting particle model is relatively simple, which allows us to derive analytic results. Many extensions of this approach are possible, and we have presented a straightforward extension to clusters of cells that cohere via co-attraction. Other variants of stochastic particle models have been used to model collective cell migration [37, 46, 50–55], though not cluster chemotaxis. Our model could be improved for quantitative comparisons by careful measurement of single-cell statistics in or out of a chemoattractant gradient [19, 56]; this could lead to nonlinear or anisotropic terms in Eq. 2. Our description of contact inhibition of locomotion has also assumed, for simplicity, that contact with both the front and back of the cell is inhibitory; other possibilities may alter the collective dynamics of the cell cluster [13].

### Distinguishing between different models for collective chemotaxis

Our model explains how chemotaxis can emerge from the interactions of non-chemotaxing cells. However, other possibilities exist for enhancement of chemotaxis in clusters. Coburn et al. showed that in contact-based models, a few chemotactic cells can direct many non-chemotactic ones [57]. If single cells are weakly chemotactic, cell-cell interactions could amplify this or simply average out fluctuations [18]. How can we distinguish these options? In Fig. 3, at large cluster sizes, the velocity saturates, and the chemotactic index saturates to one. However, these large-size results are insufficient to convincingly argue for emergent chemotaxis. As an alternate theory, suppose that each cell chemotaxes noisily, having a polarity  $\mathbf{p}^i = p_0 \nabla S + \Delta^i$ , where  $\Delta^i$  are independent zero-mean noises. In this case, assuming a rigid cluster,  $\langle \mathbf{V} \rangle = p_0 \nabla S$  independent of  $N$ , and  $\langle (V_\mu - \langle V_\mu \rangle)^2 \rangle \sim 1/N$ , very similar to our large- $N$  asymptotic results, and the circular-cluster theory of Malet-Engra et al. [4]. (We note this is not, however, a plausible explanation for the results of [4], who simultaneously ob-

serve single cell chemorepulsion and cluster chemoattraction.) In general, we argue that small-cluster-size and geometric effects are the best test of emergent chemotaxis. In particular, studying the chemotaxis of cell pairs as in Fig. 2 is an important and generic sign of cluster-level gradient sensing. Even beyond our model, chemotactic drift will be anisotropic for almost all mechanisms where single cells do not chemotax: two cells separated perpendicular to the gradient sense the same concentration. This leads to anisotropic chemotaxis as long as cells are not integrating information over times much larger than the time for the pair to reorient. By contrast, the simple model with single cell chemotaxis above leads to isotropic chemotaxis of pairs.

We observed the anisotropic chemotaxis of cell pairs in our model by studying the dynamics of many cell pairs over a long period of time, allowing us to sample many orientations and correlate them with cell pair velocities. However, tracking over long times and large numbers is naturally more challenging in experimental measurements. This problem could potentially be alleviated by studying cell pairs released from confinement in the presence of a chemoattractant gradient. Using either a narrow microstencil [41] or a dynamically patterned adhesive micropattern [58] could allow for the creation of anisotropic cell clusters and cell pairs with an established orientation. This sort of experiment would also have the advantage of the improved reliability of micropattern-based studies [21, 59].

### Summary

We have developed a simple quantitative model of collective guidance in cell clusters [3, 6] and shown that collective chemotaxis may emerge robustly even when single cells do not chemotax at all. Our work allows us to make two relatively unambiguous predictions for emergent collective guidance: 1) pairs of cells will develop anisotropic chemotaxis, and 2) because the mechanism we study is driven by the cluster edge, increasingly large strongly adherent clusters will either scatter or decrease in velocity.

## MATERIALS AND METHODS

### Computational modeling

We solve the model equations Eqs. 1-2 numerically using a standard Euler-Maruyama scheme. Throughout this paper, we choose units such that the equilibrium cell-cell separation (roughly  $20 \mu\text{m}$  for neural crest [3]) is unity, and the relaxation time  $\tau = 1$  ( $\tau$  can be estimated to be 20 minutes in neural crest [3]). Within these units, neural crest cell velocities are on the order of 1, so we choose  $\sigma = 1$ .

We adapt the cell-cell force from [51]

$$\mathbf{F}^{ij} = \hat{\mathbf{r}}^{ij} \begin{cases} v_r (d^{ij} - 1), & d^{ij} < 1 \\ v_a \frac{d^{ij} - 1}{D_0 - 1}, & 1 \leq d^{ij} < D_0 \\ 0 & d^{ij} > D_0 \end{cases} \quad (13)$$

where  $d^{ij} = |\mathbf{r}^i - \mathbf{r}^j|$ . This force is a repulsive spring below the equilibrium separation, an attractive spring above it, and vanishes above  $D_0$ .  $D_0 = 1.2$  in all of our simulations, and for the rigid-cluster simulations we use  $v_r = v_a = 500$  unless noted elsewhere.

When we include adaptation, we assume that the kinetics of Eq. 7 and Eq. 9 are fast compared with the dynamics of interest, and set them to their steady states, assuming  $k_{-R} \gg k_R$  and thus  $R^i = A^{i,ss}/I^i(t)$ . We solve Eq. 8 for  $I^i(t)$  with an Euler scheme. We set  $k_D = 4$  and  $k_I = k_{-I} = 1$  in our units. A complete list of parameters is included in the *Appendix*, Table A1.

### ACKNOWLEDGMENTS

BAC appreciates helpful discussions with Albert Bae and Monica Skoge. This work was supported by NIH Grant No. P01 GM078586, NSF Grant No. DMS 1309542, and by the Center for Theoretical Biological Physics. BAC was supported by NIH Grant No. F32GM110983.

## APPENDIX

Cluster chemotaxis when chemoattractant regulates cell persistence  $\tau$ 

Within the main paper, we have assumed that the chemoattractant concentration  $S(\mathbf{r})$  regulates the susceptibility of a cell to contact inhibition of locomotion  $\beta^i$ , with  $\beta^i = \bar{\beta}S(\mathbf{r}^i)$ . This models the stabilization of protrusions induced by contact interactions. This is consistent with the results of Theveneau et al. [3], who find that protrusion stabilization is stronger in clusters than in single cells. However, very similar results can be found if we assume that  $\beta$  is constant and the signal regulates the time required for the cell's polarity to relax, i.e.  $\tau^i = \bar{\tau}S(\mathbf{r})$ . In this case, the mean polarity of a cell is  $\langle \mathbf{p}^i \rangle = \beta \tau^i \sum_{j \sim i} \hat{\mathbf{r}}^{ij}$  and we find

$$\langle \mathbf{V} \rangle \approx \beta \bar{\tau} \mathcal{M} \cdot \nabla S \quad (\tau \text{ regulation}) \quad (\text{A1})$$

where the mobility matrix  $\mathcal{M}$  is the same as in the main paper,  $\mathcal{M}_{\mu\nu} = \frac{1}{N} \sum_i r_\nu^i q_\mu^i$ . However, because  $\tau$  varies over space, the fluctuations will also vary:  $\langle (V_\mu - \langle V_\mu \rangle)^2 \rangle = \sigma^2 N^{-2} \sum_i \tau^i = \sigma^2 N^{-1} \bar{\tau} \bar{S}$ , where  $\bar{S} = N^{-1} \sum_i S(\mathbf{r}^i)$  is the mean signal across the cluster. For this reason, the chemotactic index in the  $\tau$ -regulation model will depend on  $\nabla S / \bar{S}^{1/2}$ , and will not be constant over a linear gradient.

In addition, a single cell with a persistence time  $\tau$  that depends on the chemoattractant level will undergo biased motion. This is shown in Fig. A1 below. This drift can be made smaller than the CIL-driven cluster drift, as it is independent of  $\beta$ , while the cluster drift is proportional to  $\beta$ .

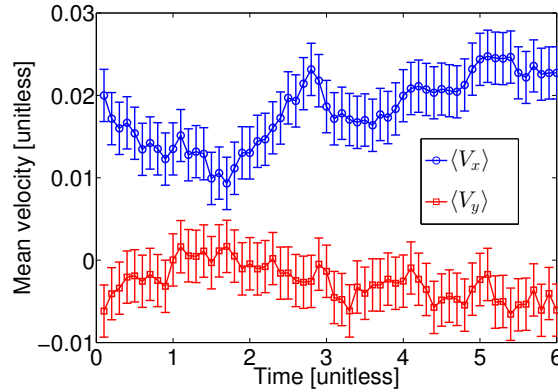


FIG. A1. **Single cells in a spatially-varying  $\tau$  develop a mean drift.** The mean  $x$  and  $y$  velocities for a cell with spatially varying  $\tau$  are shown:  $\tau = \bar{\tau}(S_0 + |\nabla S|x)$ , with  $\bar{\tau} = 1$ ,  $S_0 = 1$ ,  $|\nabla S| = 0.025$ . Result is average over  $n = 10^5$  iterations, each started at the origin; error bars indicate  $\langle [V_\mu(t) - \langle V_\mu(t) \rangle]^2 \rangle / \sqrt{n}$ .

Derivation of the  $Q$ -layer oligomer mobility matrix

We can compute the mobility matrix of the  $Q$ -layer oligomers for arbitrary  $Q$ . Our mobility matrix is given by

$$\mathcal{M}_{\mu\nu} = \frac{1}{N} \sum_i q_\mu^i r_\nu^i$$

with  $\mathbf{q}^i = \sum_{j \sim i} \hat{\mathbf{r}}^{ij}$ . To simplify the calculation, we can make a few assumptions. First, we note that  $\mathcal{M}_{xx} = \mathcal{M}_{yy}$ , but  $\mathcal{M}_{xy} = \mathcal{M}_{yx} = 0$  for the  $Q$ -layer oligomer. We only need to calculate  $\bar{\mathcal{M}} = \frac{1}{2}(\mathcal{M}_{xx} + \mathcal{M}_{yy})$ . The only cells  $i$  in the sum of Eq. 5 that are nonzero are those around the boundary.  $\bar{\mathcal{M}}$  does not depend on orientation, so we can compute the sum  $\sum_i \mathbf{r}^i \mathbf{q}^i$  for one face of the oligomer (Fig. A2), then multiply by six. However, this double-counts the corner cells, so we must weight them by  $1/2$ . We then find  $\bar{\mathcal{M}} = [\frac{9}{2}Q^2 + \frac{3}{2}Q] / N(Q)$ , where  $N(Q) = 1 + 3Q + 3Q^2$  is the number of cells in the cluster.

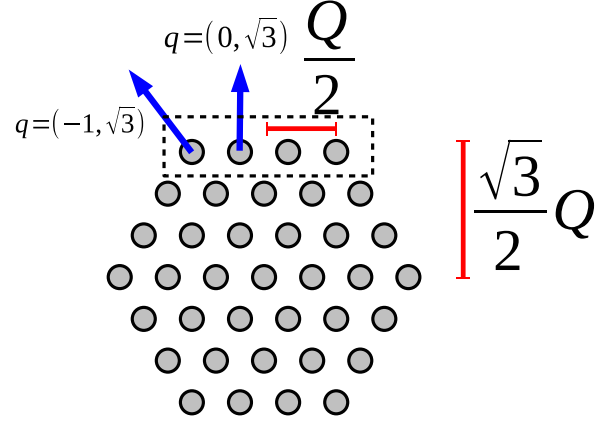


FIG. A2. Geometry of  $Q$ -layer oligomer, illustrated for  $Q = 3$ . The top face is highlighted by a dashed line.

### Rotational transformation and averaging of the mobility matrix

We can compute the mobility matrix of a rotated cluster of arbitrary shape from Eq. 5. If we rotate our cluster, which we assume is centered at the origin, by an angle  $\theta$ ,  $(\mathbf{r}^i)' = \mathcal{R}(\theta)\mathbf{r}^i$ , we find that

$$\mathcal{M}'_{\mu\nu} = \mathcal{R}_{\mu\alpha}(\theta)\mathcal{M}_{\alpha\beta}\mathcal{R}_{\nu\beta}(\theta) \quad (\text{A2})$$

where we have assumed the Einstein summation convention and  $\mathcal{R}(\theta)$  is the rotation matrix  $\begin{pmatrix} \cos\theta & -\sin\theta \\ \sin\theta & \cos\theta \end{pmatrix}$ . In matrix terms,  $\mathcal{M}' = \mathcal{R}(\theta) \cdot \mathcal{M} \cdot [\mathcal{R}(\theta)]^T$ . If we average over  $\theta$ , we find

$$\frac{1}{2\pi} \int_0^{2\pi} d\theta \mathcal{M}'(\theta) = \frac{1}{2} \begin{pmatrix} \mathcal{M}_{xx} + \mathcal{M}_{yy} & \mathcal{M}_{xy} - \mathcal{M}_{yx} \\ \mathcal{M}_{yx} - \mathcal{M}_{xy} & \mathcal{M}_{xx} + \mathcal{M}_{yy} \end{pmatrix} \quad (\text{A3})$$

We can show from the definition Eq. 5 that  $\mathcal{M}_{\mu\nu} = \mathcal{M}_{\nu\mu}$ , so the off-diagonal entries of the averaged matrix are zero, and therefore  $\frac{1}{2\pi} \int_0^{2\pi} d\theta \mathcal{M}'_{\mu\nu}(\theta) = \frac{1}{2}(\mathcal{M}_{xx} + \mathcal{M}_{yy})\delta_{\mu\nu}$ . In other words, when averaged over orientation, a cell cluster's mobility matrix is just the constant  $\overline{\mathcal{M}}$  times the identity.

### Computing the chemotactic index

We showed in the main paper that within our model, assuming that the cluster rearrangement is slow with respect to the polarity dynamics and thus each cell's polarity is given by a biased Ornstein-Uhlenbeck process, the velocity of a rigid cell cluster is

$$\mathbf{V} = \langle \mathbf{V} \rangle + \Delta \quad (\text{A4})$$

where  $\Delta$  is a Gaussian random variable with zero mean and variance  $\langle \Delta_\mu \Delta_\nu \rangle = \Gamma^2 \delta_{\mu\nu}$ . We want to compute the chemotactic index,  $CI$ ; assuming the gradient is increasing in the  $x$  direction, this is

$$CI = \frac{\langle V_x \rangle}{\langle |\mathbf{V}| \rangle} \quad (\text{A5})$$

where the average is both over time and over many trajectories. We note that this is a useful definition for us because, in our minimal model, neither  $\langle \mathbf{V} \rangle$  nor  $\Delta$  depend on the absolute value of the chemoattractant  $S$ . More care must be taken in other cases, such as the adaptation case, where in a linear gradient, the velocity will depend on the position along the gradient and thus on time. To compute  $CI$ , we need to compute  $\langle |\mathbf{V}| \rangle$ .  $|\mathbf{V}|$  is, in our case, given by a Rice

distribution, and this moment can be calculated.

$$\langle |\mathbf{V}| \rangle = \langle \sqrt{(\langle V_x \rangle + \Delta_x)^2 (\langle V_y \rangle + \Delta_y)^2} \rangle \quad (\text{A6})$$

$$= \frac{1}{2\pi\Gamma^2} \int d\Delta_x d\Delta_y \sqrt{(\langle V_x \rangle + \Delta_x)^2 + (\langle V_y \rangle + \Delta_y)^2} \exp \left[ \frac{-(\Delta_x^2 + \Delta_y^2)}{2\Gamma^2} \right] \quad (\text{A7})$$

$$= \frac{1}{2\pi\Gamma^2} \int dV_x dV_y V \exp \left[ -\frac{1}{2\Gamma^2} \{ (V_x - \langle V_x \rangle)^2 + (V_y - \langle V_y \rangle)^2 \} \right] \quad (\text{A8})$$

where  $V = \sqrt{V_x^2 + V_y^2}$ . We now switch to polar coordinates,  $V_x = V \cos \phi$ ,  $V_y = V \sin \phi$ , and correspondingly write  $\langle V_x \rangle = \nu \cos \theta$  and  $\langle V_y \rangle = \nu \sin \theta$ , where  $\nu^2 = \langle V_x \rangle^2 + \langle V_y \rangle^2$ . Thus,

$$\langle |\mathbf{V}| \rangle = \frac{1}{2\pi\Gamma^2} \int_0^{2\pi} d\phi \int_0^\infty dV V^2 \exp \left[ -\frac{1}{2\Gamma^2} \{ V^2 + \nu^2 - 2V\nu \cos(\theta - \phi) \} \right] \quad (\text{A9})$$

$$= \frac{1}{\Gamma^2} \int_0^\infty dV V^2 \exp \left[ -\frac{1}{2\Gamma^2} (V^2 + \nu^2) \right] I_0 (V\nu/\Gamma^2) \quad (\text{A10})$$

where  $I_0(x)$  is the modified Bessel function of the first kind. This integral may be evaluated, resulting in

$$\langle |\mathbf{V}| \rangle = \Gamma \sqrt{\pi/2} L_{1/2}(-\nu^2/2\Gamma^2) \quad (\text{A11})$$

where the generalized Laguerre polynomial  $L_{1/2}$  is given by

$$L_{1/2}(x) = e^{x/2} [(1-x)I_0(-x/2) - xI_1(-x/2)]. \quad (\text{A12})$$

Within our average over trajectories, we are averaging over the orientation of the cluster; thus we expect  $\langle V_y \rangle = 0$  for a chemoattractant gradient in the  $x$  direction, and  $\nu = \langle V_x \rangle = \bar{\beta}\tau\bar{\mathcal{M}}\partial_x S$ .  $\Gamma^2 = \langle (V_x - \langle V_x \rangle)^2 \rangle = \langle (V_y - \langle V_y \rangle)^2 \rangle = \sigma^2\tau/N$ . This leads to the result stated in the main paper,

$$CI = \sqrt{2/\pi} c / L_{1/2}(-c^2/2) \quad (\text{A13})$$

$$c = \frac{\langle V_x \rangle}{\sqrt{\langle (V_\mu - \langle V_\mu \rangle)^2 \rangle}} = \frac{\bar{\beta}\tau\bar{\mathcal{M}}\partial_x S}{\sigma\sqrt{\tau/N}}$$

where in our notation, we could also write  $c = \nu/\Gamma$ . We plot the result of Eq. 6 in Fig. A3 below; we see that  $CI \rightarrow 1$  as  $c \gg 1$  (corresponding to cluster velocities much larger than the noise in cluster velocity) and  $CI \rightarrow 0$  if  $|c| \ll 1$  (cluster velocity much smaller than the noise). We also note that chemotaxis could oppose the direction of the gradient (chemorepulsion) – in this case,  $CI(-c) = -CI(c)$ .

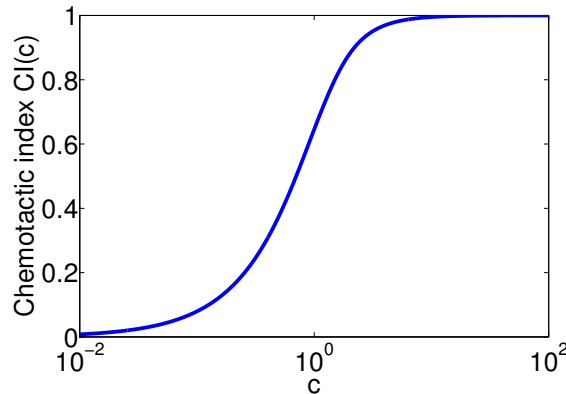


FIG. A3. Chemotactic index  $CI$  as a function of the parameter  $c$ .

### Velocity and CI of irregular clusters

In the main paper, we presented results on the velocity and chemotactic index of  $Q$ -layer oligomers. Here, we show the velocity and chemotactic index of imperfect clusters. We begin with a  $Q$ -layer oligomer, and then remove  $n$  cells at random from the outer layer; this process is repeated 200 times for each  $n$  from 1 to  $6Q$  (the number of cells in the outer layer). An example is presented in Fig. A4, with  $Q = 5$  and  $n = 5$  cells removed. The mobility matrix is computed for each cluster, and used to compute  $\langle V_x \rangle$  and  $CI$  (Fig. A4). We see that though different configurations can lead to different mean velocities for the same number of cells, the general trend is captured by the results for intact oligomers (dashed line and square symbols in Fig. A4).

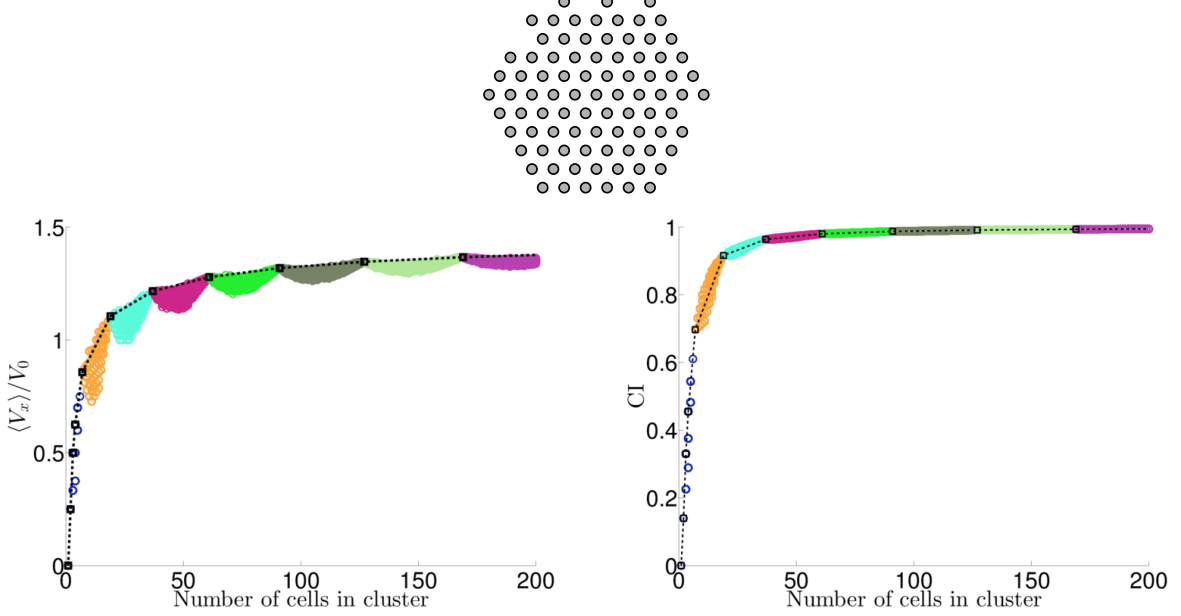


FIG. A4. **Cluster shape effects, in addition to cell number, can affect velocity and  $CI$ .** Top: illustration of  $Q$ -layer oligomer with a few cells removed from the external layer. Bottom: Velocity and chemotactic index for clusters of different shapes. Different colors indicate the size of the base cluster from which cells are removed. Black squares connected by dashed lines show the results for intact oligomers. For the  $CI$  plot, we apply our usual parameters and  $|\nabla S| = 0.025$ . All results in this figure are theoretical results for rigid clusters only, not full simulations.

### Transient rotation in the minimal model

Though we have primarily focused on the translational motion of the cluster, rotational motion can also occur in our simplest model, both through rotational diffusion and biased motion. We can analyze this by determining the net “torque”  $L_z = \sum_i [\delta \mathbf{r}^i \times \mathbf{p}^i]_z$  applied to the cluster by the cells’ traction. This torque is, on average,

$$\langle L_z \rangle = \sum_i \bar{\beta} \tau S(\mathbf{r}^i) [\delta \mathbf{r}^i \times \mathbf{q}^i]_z \quad (\text{A14})$$

where  $\mathbf{q}^i = \sum_{j \sim i} \hat{\mathbf{r}}^{ij}$  and  $\delta \mathbf{r}^i = \mathbf{r}^i - \mathbf{r}_{\text{cm}}$  is the displacement from the cluster center of mass.

What torque is required to cause the cluster to move at a fixed angular velocity? For a cluster moving in a rigid rotation with angular velocity  $\Omega$ , the cell velocities are  $\mathbf{v}^i = \Omega (-\delta r_y^i, \delta r_x^i)$ . To achieve this, each cell must have a polarity of  $\mathbf{p}^i = \Omega (-\delta r_y^i, \delta r_x^i)$ , leading to  $L_z = \Omega \sum_i |\delta \mathbf{r}^i|^2$ . The angular velocity is thus related to  $L_z$  by  $\Omega = L_z / \sum_i |\delta \mathbf{r}^i|^2$ . We thus find, for linear gradients,  $S = S_0 + \mathbf{r} \cdot \nabla S$ ,

$$\langle \Omega \rangle = \bar{\beta} \tau \mathbf{A} \cdot \nabla S \quad (\text{A15})$$

where the vector  $\mathbf{A}$  only depends on the cluster geometry,

$$\mathbf{A} = \frac{\sum_i \delta \mathbf{r}^i [\delta \mathbf{r}^i \times \mathbf{q}^i]_z}{\sum_i |\delta \mathbf{r}^i|^2} \quad (\text{A16})$$

where  $\mathbf{q}^i$  is defined as above. (Note that  $\sum_i \delta \mathbf{r}^i \times \mathbf{q}^i = \sum_i \mathbf{r}^i \times \mathbf{q}^i = -\sum_{i,j \sim i} \frac{\mathbf{r}^i \times \mathbf{r}^j}{|\mathbf{r}^i - \mathbf{r}^j|} = 0$ , allowing us to drop a center of mass term.) For all of the shapes listed in Table I in the main paper,  $\mathbf{A} = \mathbf{0}$ . Cell clusters must lack an inversion symmetry to be rotated by the gradient.

However, even if  $\mathbf{A} \neq \mathbf{0}$ , clusters will not persistently rotate. We can see that if we rotate the cell cluster around its center of mass,  $\mathbf{A}$  must also rotate as a vector. If the gradient is along the  $x$  direction, this lets us write  $\langle \Omega \rangle = \langle \dot{\theta} \rangle = \bar{\beta} \tau [A_x(0) \cos \theta - A_y(0) \sin \theta]$ , where  $\mathbf{A}(0)$  is Eq. A16 calculated for a reference geometry. We see that if  $\mathbf{A} \neq \mathbf{0}$ , the cluster will rotate to a stable angle  $\theta^*$  given by  $\tan \theta^* = A_x(0)/A_y(0)$ . In a linear gradient, there is no persistent rotation.

We note that Eq. A15 is not as quantitatively accurate as the corresponding result for translational motion, at least for the parameter set in the main paper; this occurs because a small deviation from the equilibrium polarity  $\langle \mathbf{p}^i \rangle$  can create a relatively large change in torque. It will be more accurate for systems where the relaxation time  $\tau$  is smaller compared to the rotational motion of the cluster.

### Proof of perfect adaptation and gradient sensing in limit $k_{-I}/k_D \ll 1$

Our reaction-diffusion model for inhibitor, activator, and response on our network of cells is a direct application of the model of [16] to a network of cells,

$$\partial_t A^i = k_A S(\mathbf{r}^i) - k_{-A} A^i \quad (\text{A17})$$

$$\partial_t I^i = k_I S(\mathbf{r}^i) - k_{-I} I^i - k_D n^i I^i + k_D \sum_{j \sim i} I^j \quad (\text{A18})$$

$$\partial_t R^i = k_R A^i (1 - R^i) - k_{-R} I^i R^i \quad (\text{A19})$$

The steady states of Eq. 7 and Eq. A19 are  $A^{i,ss} = \frac{k_A}{k_{-A}} S^i$  and  $R^{i,ss} = \frac{A^i/I^i}{A^i/I^i + k_{-R}/k_R}$ .

If the signal is constant, the response steady state is independent of the signal: we can see that if  $S(\mathbf{r}) = S_0$ ,  $I^{i,ss} = I^{ss}$ , and that  $I^{i,ss} = \frac{k_I}{k_{-I}} S_0$  and thus  $A^{i,ss}/I^{i,ss} = \frac{k_A}{k_{-A}} \frac{k_{-I}}{k_I}$ , independent of  $S_0$ .

If the signal is *not* uniform, we can find the steady state of Eq. A18 perturbatively in the limit of  $\alpha \equiv k_{-I}/k_D \ll 1$ . Defining  $\iota = k_I/k_{-I}$ , we find that the steady state of Eq. A18 obeys

$$\iota \alpha S(\mathbf{r}^i) - \alpha I^{i,ss} + \sum_j \mathcal{L}^{ij} I^{j,ss} = 0 \quad (\text{A20})$$

where  $\mathcal{L}^{ij} = C^{ij} - n^i \delta^{ij}$ , where  $C^{ij}$  is the adjacency matrix of the graph representing cell connections, i.e.  $C^{ij} = 1$  if  $i \sim j$  and 0 otherwise.  $\mathcal{L}^{ij}$  is the “network Laplacian” of the graph [29]. We note that  $\sum_j \mathcal{L}^{ij} = \sum_i \mathcal{L}^{ij} = 0$ .  $\mathcal{L}^{ij}$  is also a W-matrix [20], and by the properties of W-matrices will have a unique (up to normalization) zero eigenvector  $\sum_j \mathcal{L}^{ij} V^j = 0$ , assuming that the cell cluster is connected. This eigenvector will be constant,  $V^j = 1$ .

If we write  $I^{i,ss} = I_{(0)}^{i,ss} + \alpha I_{(1)}^{i,ss} + \dots$ , by equating powers of  $\alpha$  we find that

$$\sum_j \mathcal{L}^{ij} I_{(0)}^{j,ss} = 0 \quad (\text{Zeroth order in } \alpha) \quad (\text{A21})$$

$$\iota S(\mathbf{r}^i) - I_{(0)}^{i,ss} + \sum_j \mathcal{L}^{ij} I_{(1)}^{j,ss} = 0 \quad (\text{First order in } \alpha) \quad (\text{A22})$$

We see from Eq. A21 and the properties of the network Laplacian discussed above that the zeroth order solution  $I_{(0)}^{i,ss}$  must be a constant -  $I_{(0)}^{i,ss} = \bar{I}$ . We can set the overall value of that constant by summing Eq. A22 over  $i$ .  $\sum_i \mathcal{L}^{ij} = 0$ , leading us to conclude

$$\bar{I} = I_{(0)}^{i,ss} = \frac{\iota}{N} \sum_i S(\mathbf{r}^i) = \iota \bar{S} \quad (\text{A23})$$

where  $\bar{S}$  is the mean value of  $S$  over the cluster. This result, combined with the steady-state for  $A$  and the assumption that  $R^{i,ss} = \frac{A^i/I^i}{A^i/I^i + k_{-R}/k_R} \approx \frac{k_R}{k_{-R}} \frac{A^i}{I^i}$  yields

$$R^{i,ss} \approx \frac{k_R}{k_{-R}} \frac{k_A}{k_{-A}} \frac{k_{-I}}{k_I} \frac{S(\mathbf{r}^i)}{\bar{S}} \equiv R_0 \frac{S(\mathbf{r}^i)}{\bar{S}} \quad (\text{A24})$$

as quoted in the main paper.

When can this be applied? We expect that in a time  $t$ ,  $I$  will diffuse over  $\sim k_D t$  cells; we expect then that if  $I$  equilibrates over the cluster within the time scale  $1/k_{-I}$ , or  $k_D/k_{-I} \gg N$ , we should have good gradient sensing. This implies that  $\alpha \ll N^{-1}$  for observing linear gradient sensing. This is merely the cell-level version of the conditions applied for the simple one-dimensional gradient sensing module presented in in [16].

### Details of co-attraction model

We assume that cells secrete a chemical with concentration  $c$ , which diffuses in a the extracellular medium with a diffusion coefficient  $D$ , and breaks down with a rate  $k_c$ . For a single cell at the origin, the equation for  $c(\mathbf{r})$  is then:

$$\partial_t c(\mathbf{r}, t) = D\nabla^2 c - k_c c + s\delta(\mathbf{r}) \quad (\text{A25})$$

where  $s$  is the secretion rate. We assume that the chemical reaches steady state,  $\partial_t c = 0$ . We can solve this equation via Fourier transformation, finding that (treating our system as two-dimensional)

$$c(\mathbf{r}) = \frac{s}{2\pi D} K_0(r/\ell) \quad (\text{A26})$$

where  $\ell^2 = D/k_c$  and  $K_0(x)$  is the modified Bessel function of the second kind. By superimposing many solutions, we find that for cells at positions  $\mathbf{r}^i$ ,

$$c(\mathbf{r}^i) = \frac{s}{2\pi D} \sum_j K_0(|\mathbf{r}^i - \mathbf{r}^j|/\ell) \quad (\text{A27})$$

Taking the gradient of this, we find (ignoring the singularity when  $i = j$ )

$$\nabla c(\mathbf{r}^i) = -\frac{s}{2\pi D\ell} \sum_{j \neq i} K_1(|\mathbf{r}^i - \mathbf{r}^j|/\ell) \hat{\mathbf{r}}^{ij} \quad (\text{A28})$$

We choose  $s = 2\pi D\ell$  without loss of generality; this parameter could also be rescaled into the value of  $\chi$ .

### Table of parameters

Parameter symbol	Name	Value in our units
$\tau$	Persistence time	1
$\sigma$	Characteristic cell speed (OU noise parameter)	1
$\bar{\beta}$	CIL strength	20 (or as noted)
$v_a$	Adhesion strength	500 (or as noted)
$v_r$	Cell repulsion strength	500 (or as noted)
$D_0$	Maximum interaction length	1.2
$k_A, k_{-A}$	LEGI activator rates	Assumed fast (see <i>Methods</i> )
$k_R, k_{-R}$	LEGI response rates	Assumed fast (see <i>Methods</i> )
$k_I, k_{-I}$	LEGI inhibitor rates	1
$k_D$	Cell-cell diffusion rate	4
$\xi$	Amplification switch threshold	0.01
$S_0$	Signal strength at origin	1
$\ell$	Degradation length	5
$g_0$	Gradient threshold value	$10^{-5}$
$\Delta t$	Time step	$10^{-4}$ for rigid simulations, 0.005 for co-attraction

TABLE A1. Parameters used



- [1] Herbert Levine and Wouter-Jan Rappel. The physics of eukaryotic chemotaxis. *Physics Today*, 66(2), 2013.
- [2] Jeffrey E Segall, Steven M Block, and Howard C Berg. Temporal comparisons in bacterial chemotaxis. *Proceedings of the National Academy of Sciences*, 83(23):8987, 1986.
- [3] Eric Theveneau, Lorena Marchant, Sei Kuriyama, Mazhar Gull, Barbara Moepps, Maddy Parsons, and Roberto Mayor. Collective chemotaxis requires contact-dependent cell polarity. *Developmental Cell*, 19(1):39, 2010.
- [4] Gema Malet-Engra, Weimiao Yu, Amanda Oldani, Javier Rey-Barroso, Nir S Gov, Giorgio Scita, and Loïc Dupré. Collective cell motility promotes chemotactic prowess and resistance to chemorepulsion. *Current Biology*, 25:242, 2015.
- [5] Ambra Bianco, Minna Poukkula, Adam Cliffe, Juliette Mathieu, Carlos M Luque, Tudor A Fulga, and Pernille Rørth. Two distinct modes of guidance signalling during collective migration of border cells. *Nature*, 448(7151):362, 2007.
- [6] Pernille Rørth. Collective guidance of collective cell migration. *Trends in Cell Biology*, 17(12):575, 2007.
- [7] Mikiko Inaki, Smitha Vishnu, Adam Cliffe, and Pernille Rørth. Effective guidance of collective migration based on differences in cell states. *Proceedings of the National Academy of Sciences*, 109(6):2027, 2012.
- [8] Xiaobo Wang, Li He, Yi I Wu, Klaus M Hahn, and Denise J Montell. Light-mediated activation reveals a key role for rac in collective guidance of cell movement in vivo. *Nature Cell Biology*, 12(6):591, 2010.
- [9] Andrew Berdahl, Colin J Torney, Christos C Ioannou, Jolyon J Faria, and Iain D Couzin. Emergent sensing of complex environments by mobile animal groups. *Science*, 339(6119):574, 2013.
- [10] Nicola Aceto, Aditya Bardia, David T Miyamoto, Maria C Donaldson, Ben S Wittner, Joel A Spencer, Min Yu, Adam Pely, Amanda Engstrom, Huili Zhu, et al. Circulating tumor cell clusters are oligoclonal precursors of breast cancer metastasis. *Cell*, 158(5):1110, 2014.
- [11] Carlos Carmona-Fontaine, Helen K Matthews, Sei Kuriyama, Mauricio Moreno, Graham A Dunn, Maddy Parsons, Claudio D Stern, and Roberto Mayor. Contact inhibition of locomotion in vivo controls neural crest directional migration. *Nature*, 456(7224):957, 2008.
- [12] Roberto Mayor and Carlos Carmona-Fontaine. Keeping in touch with contact inhibition of locomotion. *Trends in Cell Biology*, 20(6):319, 2010.
- [13] Brian A Camley, Yunsong Zhang, Yanxiang Zhao, Bo Li, Eshel Ben-Jacob, Herbert Levine, and Wouter-Jan Rappel. Polarity mechanisms such as contact inhibition of locomotion regulate persistent rotational motion of mammalian cells on micropatterns. *Proceedings of the National Academy of Sciences*, 111(41):14770, 2014.
- [14] M Abercrombie. Contact inhibition and malignancy. *Nature*, 281(5729):259, 1979.
- [15] Ravi A Desai, Smitha B Gopal, Sophia Chen, and Christopher S Chen. Contact inhibition of locomotion probabilities drive solitary versus collective cell migration. *Journal of The Royal Society Interface*, 10(88):20130717, 2013.
- [16] Andre Levchenko and Pablo A Iglesias. Models of eukaryotic gradient sensing: application to chemotaxis of amoebae and neutrophils. *Biophysical Journal*, 82(1):50, 2002.
- [17] Carlos Carmona-Fontaine, Eric Theveneau, Apostolia Tzekou, Masazumi Tada, Mae Woods, Karen M Page, Maddy Parsons, John D Lambris, and Roberto Mayor. Complement fragment c3a controls mutual cell attraction during collective cell migration. *Developmental Cell*, 21(6):1026, 2011.
- [18] Andrew M Simons. Many wrongs: the advantage of group navigation. *Trends in Ecology & Evolution*, 19(9):453, 2004.
- [19] David Selmecki, Stephan Mosler, Peter H Hagedorn, Niels B Larsen, and Henrik Flyvbjerg. Cell motility as persistent random motion: theories from experiments. *Biophysical Journal*, 89(2):912, 2005.
- [20] Nicolaas Godfried Van Kampen. *Stochastic processes in physics and chemistry*, volume 1. Elsevier, 1992.
- [21] Benjamin Lin, Taofei Yin, Yi I Wu, Takanari Inoue, and Andre Levchenko. Interplay between chemotaxis and contact inhibition of locomotion determines exploratory cell migration. *Nature communications*, 6, 2015.
- [22] Sangtae Kim and Seppo J Karrila. *Microhydrodynamics: principles and selected applications*. Courier Dover Publications, 2013.
- [23] Yilong Han, AM Alsayed, Maurizio Nobili, Jian Zhang, Tom C Lubensky, and Arjun G Yodh. Brownian motion of an ellipsoid. *Science*, 314(5799):626, 2006.
- [24] Danny Fuller, Wen Chen, Micha Adler, Alex Groisman, Herbert Levine, Wouter-Jan Rappel, and William F Loomis. External and internal constraints on eukaryotic chemotaxis. *Proceedings of the National Academy of Sciences*, 107(21):9656, 2010.
- [25] Tau-Mu Yi, Yun Huang, Melvin I Simon, and John Doyle. Robust perfect adaptation in bacterial chemotaxis through integral feedback control. *Proceedings of the National Academy of Sciences*, 97(9):4649, 2000.
- [26] Kosuke Takeda, Danying Shao, Micha Adler, Pascale G Charest, William F Loomis, Herbert Levine, Alex Groisman, Wouter-Jan Rappel, and Richard A Firtel. Incoherent feedforward control governs adaptation of activated ras in a eukaryotic chemotaxis pathway. *Science Signaling*, 5(205):ra2, 2012.
- [27] Monica Skoge, Haicen Yue, Michael Erickstad, Albert Bae, Herbert Levine, Alex Groisman, William F Loomis, and Wouter-Jan Rappel. Cellular memory in eukaryotic chemotaxis. *Proceedings of the National Academy of Sciences*, 111(40):14448, 2014.
- [28] Yuan Xiong, Chuan-Hsiang Huang, Pablo A Iglesias, and Peter N Devreotes. Cells navigate with a local-excitation, global-inhibition-biased excitable network. *Proceedings of the National Academy of Sciences*, 107(40):17079, 2010.
- [29] Hiroya Nakao and Alexander S Mikhailov. Turing patterns in network-organized activator-inhibitor systems. *Nature Physics*, 6(7):544, 2010.
- [30] HG Othmer and LE Scriven. Instability and dynamic pattern in cellular networks. *Journal of Theoretical Biology*, 32(3):507, 1971.
- [31] X Xu, WEI Li, GY Huang, R Meyer, T Chen, Y Luo, MP Thomas, GL Radice, and CW Lo. Modulation of mouse neural crest cell motility by n-cadherin and connexin 43 gap junctions. *The Journal of Cell Biology*, 154(1):217, 2001.
- [32] GY Huang, ES Cooper, K Waldo, ML Kirby, NB Gilula, and CW Lo. Gap junction-mediated cell-cell communication modulates mouse neural crest migration. *The Journal of Cell Biology*, 143(6):1725, 1998.
- [33] Christopher M Waters and Bonnie L Bassler. Quorum sensing: cell-to-cell communication in bacteria. *Annu. Rev. Cell Dev. Biol.*, 21:319, 2005.
- [34] T Bollenbach, K Kruse, P Pantazis, M González-Gaitán, and F Jülicher. Robust formation of morphogen gradients. *Physical Review Letters*, 94(1):018103, 2005.
- [35] Margaret H Wade, James E Trosko, and Melvin Schindler. A fluorescence photobleaching assay of gap junction-mediated communication between human cells. *Science*, 232(4749):525, 1986.
- [36] Herbert Levine, David A Kessler, and Wouter-Jan Rappel. Directional sensing in eukaryotic chemotaxis: a balanced inactivation model. *Proceedings of the National Academy of Sciences*, 103(26):9761, 2006.
- [37] Néstor Sepúlveda, Laurence Petitjean, Olivier Cochet, Erwan Grasland-Mongrain, Pascal Silberzan, and Vincent Hakim. Collective cell motion in an epithelial sheet can be quantitatively described by a stochastic interacting particle model. *PLoS Computational Biology*, 9(3):e1002944, 2013.
- [38] Thomas E Angelini, Edouard Hannezo, Xavier Trepat, Jeffrey J Fredberg, and David A Weitz. Cell migration driven by cooperative substrate deformation patterns. *Physical Review Letters*, 104(16):168104, 2010.
- [39] Thomas E Angelini, Edouard Hannezo, Xavier Trepat, Manuel Marquez, Jeffrey J Fredberg, and David A Weitz. Glass-like dynamics of collective cell migration. *Proceedings of the National Academy of Sciences*, 108(12):4714, 2011.
- [40] Mathieu Poujade, Erwan Grasland-Mongrain, A Hertzog, J Jouanneau, P Chavrier, Benoît Ladoux, Axel Buguin, and Pascal Silberzan. Collective migration of an epithelial monolayer in response to a model wound. *Proceedings of the National Academy of Sciences*, 104(41):15988, 2007.
- [41] L Petitjean, M Reffay, E Grasland-Mongrain, M Poujade, B Ladoux, A Buguin, and P Silberzan. Velocity fields in a collectively migrating epithelium. *Biophysical Journal*, 98(9):1790, 2010.
- [42] A Szabó, R Ünneper, E Méhes, WO Twał, WS Argraves, Y Cao, and A Czirok. Collective cell motion in endothelial monolayers. *Physical*

- Biology*, 7(4):046007, 2010.
- [43] A Szabó, K Varga, T Garay, B Hegedűs, and A Cziráok. Invasion from a cell aggregate: the roles of active cell motion and mechanical equilibrium. *Physical Biology*, 9(1):016010, 2012.
- [44] Mae L Woods, Carlos Carmona-Fontaine, Chris P Barnes, Iain D Couzin, Roberto Mayor, and Karen M Page. Directional collective cell migration emerges as a property of cell interactions. *PLoS ONE*, 9(9):e104969, 2014.
- [45] Hao Yang, Xue Gou, Yong Wang, Tarek M Fahmy, Anskar Y-H Leung, Jian Lu, and Dong Sun. A dynamic model of chemoattractant-induced cell migration. *Biophysical Journal*, 108(7):1645, 2015.
- [46] András Cziráok, Eshel Ben-Jacob, Inon Cohen, and Tamás Vicsek. Formation of complex bacterial colonies via self-generated vortices. *Physical Review E*, 54(2):1791, 1996.
- [47] Herbert Levine, Wouter-Jan Rappel, and Inon Cohen. Self-organization in systems of self-propelled particles. *Physical Review E*, 63(1):017101, 2000.
- [48] Maria R D'Orsogna, Yao-Li Chuang, Andrea L Bertozzi, and Lincoln S Chayes. Self-propelled particles with soft-core interactions: patterns, stability, and collapse. *Physical Review Letters*, 96(10):104302, 2006.
- [49] Xavier Trepat, Michael R Wasserman, Thomas E Angelini, Emil Millet, David A Weitz, James P Butler, and Jeffrey J Fredberg. Physical forces during collective cell migration. *Nature Physics*, 5(6):426, 2009.
- [50] Brian A Camley and Wouter-Jan Rappel. Velocity alignment leads to high persistence in confined cells. *Physical Review E*, 89(6):062705, 2014.
- [51] Balint Szabo, GJ Szöllösi, B Gönci, Zs Jurányi, David Selmeczi, and Tamás Vicsek. Phase transition in the collective migration of tissue cells: experiment and model. *Physical Review E*, 74(6):061908, 2006.
- [52] Bo Li and Sean X Sun. Coherent motions in confluent cell monolayer sheets. *Biophysical Journal*, 107(7):1532, 2014.
- [53] Ruben van Drogen, Anshuman Pal, Carl P Goodrich, and Timon Idema. Collective dynamics of soft active particles. *Physical Review E*, 91:032706, 2015.
- [54] Markus Basan, Jens Elgeti, Edouard Hannezo, Wouter-Jan Rappel, and Herbert Levine. Alignment of cellular motility forces with tissue flow as a mechanism for efficient wound healing. *Proceedings of the National Academy of Sciences*, 110(7):2452, 2013.
- [55] Juliane Zimmermann, Ryan L Hayes, Markus Basan, José N Onuchic, Wouter-Jan Rappel, and Herbert Levine. Intercellular stress reconstitution from traction force data. *Biophysical Journal*, 107(3):548, 2014.
- [56] Gabriel Amselem, Matthias Theves, Albert Bae, Eberhard Bodenschatz, and Carsten Beta. A stochastic description of dictyostelium chemotaxis. *PLoS ONE*, 7(5):e37213, 2012.
- [57] Luke Coburn, Luca Cerone, Colin Torney, Iain D Couzin, and Zoltan Neufeld. Tactile interactions lead to coherent motion and enhanced chemotaxis of migrating cells. *Physical Biology*, 10(4):046002, 2013.
- [58] Srivatsan Raghavan, Ravi A Desai, Youngeun Kwon, Milan Mrksich, and Christopher S Chen. Micropatterned dynamically adhesive substrates for cell migration. *Langmuir*, 26(22):17733, 2010.
- [59] Elena Scarpa, Alice Roycroft, Eric Theveneau, Emmanuel Terriac, Matthieu Piel, and Roberto Mayor. A novel method to study contact inhibition of locomotion using micropatterned substrates. *Biology Open*, 2(9):901, 2013.